International Journal of Heat and Mass Transfer 145 (2019) 118676

Contents lists available at ScienceDirect

International Journal of Heat and Mass Transfer

journal homepage: www.elsevier.com/locate/ijhmt

Is a non-phase change heat pipe a new heat pipe?

Sara Kloczko [a,*], Amir Faghri [a], Yuhua Li [b]

[a] Department of Mechanical Engineering, University of Connecticut, 191 Auditorium Road, Storrs, CT 06269-3139, USA
[b] Institute of Engineering Thermophysics, Chinese Academy of Sciences, Beijing, China

ARTICLE INFO

Article history:
Received 31 May 2019
Received in revised form 31 August 2019
Accepted 31 August 2019
Available online 19 September 2019

ABSTRACT

A Non-phase change heat pipe (NPCHP) with no wick was proposed recently as a new heat pipe which is not dependent on a wick or phase change at steady state operation and where heat transfer is driven by the pressure response to a heat input, rather than phase change. The NPCHP is not a new device as suggested but is a loop thermosyphon with very high fill ratio. This effort focuses on proving the NPCHP, as an overfilled loop thermosyphon, is an effective heat transfer device through experiments and numerical simulations. An analysis of the operation and effectiveness of the device is performed, and it is shown to exhibit several heat transfer characteristics of a heat pipe, including high thermal conductivity and a fast thermal response time. Depending upon the initial fill ratio of the NPCHP, the device is shown to either operate as an overfilled two-phase loop thermosyphon or a single-phase loop thermosyphon. The NPCHP exhibits characteristics of a loop thermosyphon and can be classified as such.

1. Introduction

A heat pipe is a highly effective and well-established device which transfers a large amount of heat from one location to another. The components of a conventional heat pipe are the wick, outer wall, and working fluid, which flows through the three main sections of the heat pipe: evaporator, adiabatic section, and condenser [9]. A diagram of a conventional heat pipe is shown in Fig. 1a [3]. There is a small temperature drop between the evaporator and condenser section of the heat pipe, referred to as the adiabatic section, where the heat pipe operates nearly isothermally [10]. Heat is applied externally to the evaporator section and vaporizes the fluid in the saturated wick, which is driven by the vapor pressure through the adiabatic section to the condenser where it condenses and releases its latent heat, then is returned to the evaporator by capillary action of the wick [7,27]. The main driver of heat transfer in the conventional heat pipe is phase change and the wick. There are several different types of heat pipe depending on the application, including: conventional heat pipes, loop heat pipes (LHP), pulsating heat pipes (PHP), and thermosyphons, which can also be broken up into conventional thermosyphons and single- and two-phase loop thermosyphons. A conventional heat pipe reliant on phase change has several limits. These limits include the viscous, sonic, capillary, entrainment, flooding, and boiling limits. Challenges and opportunities of heat pipes are discussed by Faghri [8]. Heat pipe analysis and numerical simulation covering all types of heat pipes with various levels of approximation is reviewed by Bergman & Faghri [2].

A LHP is similar to a conventional heat pipe in that it uses a wick structure to help transport working fluid. Unlike the conventional heat pipe, the LHP contains a wick in the evaporator and reservoir only and forms a closed loop rather than a straight pipe and can transfer heat over long distances. The main principles of the LHP include: the use of fine-pored wicks, decrease in the distance of the liquid motion in the wick, organization of effective heat exchange during the evaporation and condensation of a working fluid, and minimal pressure losses in the adiabatic section [22]. The LHP takes heat input at the evaporator section which vaporizes the working fluid and transports it by capillary action to the condenser where it is condensed back into a liquid, releasing its latent heat. Unlike a conventional heat pipe, a LHP has a reservoir, which holds excess fluid and draws condensed liquid from the condenser back to the evaporator. The reservoir operates at a temperature slightly lower than the evaporator. Since the wick only exists in the evaporator and reservoir, the connection between the evaporator and condenser is by smooth tubes which minimizes pressure drop. The primary wick is composed of fine pores, which allows for the development of the high capillary pressure required for circulation of the fluid around the loop. A LHP can operate effectively at any orientation in the gravitational field and can transport heat over longer distances than conventional heat pipes [9].

A PHP is a closed, two-phase system capable of transporting heat from a heat source to a heat sink without any additional power input and dissipating high heat fluxes. The unique feature of PHPs, compared to conventional heat pipes, is that there is no

* Corresponding author.
E-mail address: Sara.Kloczko@uconn.edu (S. Kloczko).

https://doi.org/10.1016/j.ijheatmasstransfer.2019.118676
0017-9310/

Nomenclature

A_c	cross-sectional area (m^2)
A_s	surface area (m^2)
D	diameter (m)
h	convection coefficient (W/ m^2•K)
h	specific enthalpy (J/kg)
h	average enthalpy of multiphase mixture (J/kg)
k	thermal conductivity (W/m K)
L	length (m)
$\dot{m}$	rate of mass transfer due to evaporation or condensation (kg/s m^3)
$\dot{m}'''_{jk}$	mass transfer per unit volume from phase j to phase k due to phase change
$\dot{\mathbf{M}}'''_I$	momentum production rate due to interaction between phases along their separating interfaces $\dot{\mathbf{M}}'''_I = \sum_{k=1}^{\Pi}\sum_{j=1(j\neq k)}^{\Pi}\langle \dot{m}'''_{jk}\rangle\langle \mathbf{V}_{k,I}\rangle^k$
p	pressure (Pa)
$\mathbf{q}''$	heat flux vector (W/m^2)
q'''	Internal heat generation per unit volume (W/m^3)
Q	heat (W)
r	mass transfer intensity factor
T	temperature (K)
$\mathbf{V}$	velocity vector (m/s)
$\mathbf{V}$	mass-averaged velocity vector, $\frac{1}{\langle\rho\rangle}\left(\sum_{k=1}^{\Pi}\varepsilon_k\langle\rho_k\rangle^k\langle\mathbf{V}_k\rangle^k\right)$ (m/s)
$\mathbf{X}$	body force vector

Other

$\langle\rangle$	volume averaged
$\langle\rangle^k$	phase averaged
$\frac{D}{Dt}$	substantial derivative

Greek symbols

ε	volume fraction
Π	number of phases
ρ	density (kg/m^3)
$\boldsymbol{\tau}$	viscous stress tensor (N/m^2)
$\boldsymbol{\tau}'$	stress tensor (N/m^2)
∇	laplace operator vector

Subscript

a	adiabatic
ave	average
c	condenser
e	evaporator
eff	effective
I	interface
in	input
k	k^{th} phase
l	liquid phase
max	maximum
out	output
r	radial
sat	saturated state
v	vapor phase
∞	free stream

wick structure to return the condensate to the heating section, and therefore no countercurrent flow between the liquid and vapor [36]. PHPs have a very small diameter which allows vapor plugs and liquid slugs to form as a result of capillary action [9]. In a PHP, the liquid and vapor are distributed throughout the pipe as liquid slugs and vapor bubbles. The vapor pressure of the bubbles increases as the evaporator section of the pipe is heated, which pushes the liquid slugs toward the cooled section where the vapor bubbles condense. As the vapor bubbles condense, vapor pressure decreases and the working fluid flows back to the evaporator, creating an oscillatory flow. The driving forces of this oscillation are the surface tension, gravity, and fluctuation in pressure from the evaporator to condenser sections. Some of the major advantages of the PHP include: easy to realize miniaturization because the size of the PHP can be very small due to small inner diameter, and high flexibility because the pipe can be arranged in arbitrary configurations to match the application [14].

A two-phase conventional thermosyphon (TPCTS), a schematic of which is shown in Fig. 1b., is sometimes referred to as a gravity assisted heat pipe and consists of an evaporator and condenser. There is no wick in TPCTS because the force of gravity drives the fluid flow. The liquid and vapor occupy a single straight tube and the flow is counter-current. The heat input to the evaporator vaporizes the working fluid, which then flows up to the condenser. The working fluid is then condensed back into a liquid in the condenser section, releases its latent heat, and drains back down the walls to the evaporator.

Due to the counter-current flow of the liquid and vapor, the thermosyphon performance is limited by the flooding limit. This occurs when working fluid temperature is low, and vapor velocity is high. The shear of the vapor traveling to the condenser prevents liquid film on the wall from traveling back to the condenser. The conventional thermosyphon is also subject to the dry-out limit. This occurs when the fill charge ratio is too small and the condensate film eventually dries out [25]. Thermosyphon performance has been studied extensively, varying several parameters including: working fluid, fill ratio, heat input, and orientation. For conventional thermosyphons, fill ratio is usually described as volume of working fluid relative to the volume of the evaporator. The fill ratio is sometimes also reported as volume of working fluid relative to the total thermosyphon volume. For the experiment discussed, fill ratio is the percentage of volume filled with respect to the total volume of the loop. Working fluid is chosen based on compatibility with pipe material and other system parameters, including operating temperature. [37] tested several fill ratios between 50% and 150% of the evaporator volume and reported the optimal fill ratio to be 100% (the evaporator is initially entirely filled with working fluid), in their case water was used.

The two-phase loop thermosyphon (TPLTS), a general schematic of which is shown in Fig. 1c, consists of an evaporator, riser, condenser, and downcomer. Heat input to the evaporator section vaporizes the working fluid [35]. The vapor (or liquid-vapor mix, depending on the initial fill ratio) then flows up the riser to the condenser where it is condensed back into a liquid. The flow in the TPLTS is co-current, with liquid and vapor flowing in the same direction around the loop. The liquid phase (or liquid-vapor mix, depending on the initial fill ratio) flows down the downcomer back to the evaporator. The flow of liquid is driven by the density difference of the lower temperature fluid coming from the condenser and the higher temperature lower density flow from the evaporator [16]. The TPLTS has no flooding limit. Some TPLTS have wicks in the evaporator and some do not. However, the TPLTS operates more effectively with wick structures in the evaporator than without [15]. The TPLTS relies on gravity for the flow of working fluid, and the heat transfer relies on the heat of vaporization.

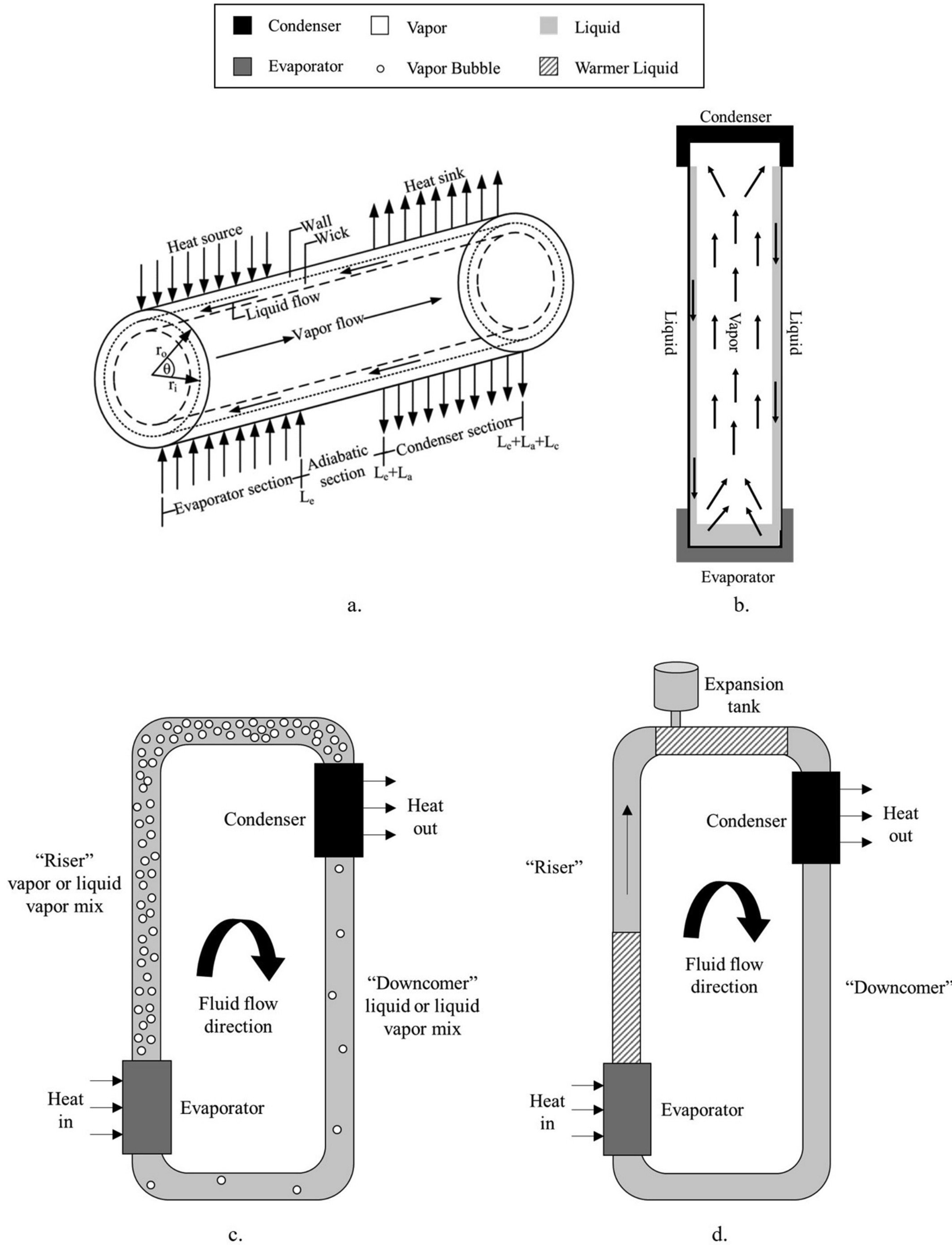

Fig. 1. Diagrams of (a). Conventional Heat Pipe (b). Two-phase Conventional Thermosyphon (c). Two-phase Loop Thermosyphon (d). Single-phase Loop Thermosyphon Showing the Flow of Liquid and/or Vapor.

Several key parameters that influence the performance of the TPLTS are: heat input, internal tube diameter, distance between evaporator and condenser, length of heat input zone, thermophysical properties of working fluid, operating pressure, and volumetric filling ratio [12]. The flow in the TPLTS is co-current, with liquid and vapor flowing in the same direction around the loop. For low fill ratios, there is no liquid in the riser (section through which vapor flows to the evaporator), and for high fill ratios, generally greater than 100% relative to the evaporator volume, there is a mixture of liquid and vapor in both the riser and the downcomer (section connecting the condenser to the evaporator through which the condensed working fluid flows) [31]. The TPLTS relies on gravity for the flow of working fluid, and the heat transfer relies on the heat of vaporization.

The ideal fill ratio depends on the boiling point and latent heat of the fluid being used. For low fill ratios, dry-out may occur for the system with wick structure [15]. The amount of working fluid is chosen such that the liquid builds up in the downcomer below the condenser, thus generating hydrostatic head in the evaporator. When water is used as the working fluid, optimal fill ratios of 30% were reported by Kang et al. [15], Chehade et al. [5] determined the optimal fill ratio to be between 7% and 10% relative to the total loop volume, and Chang et al. [4] reported an optimal fill ratio of 50% relative to the evaporator volume. Several other working fluids have been tested in TPLTS and the optimal fill ratios were determined. According to Kang et al., [15] the ideal fill ratio is 10% with methanol as the working. Naresh & Balaji [23] studied the effect of fill ratio on performance of the TPLTS and concluded the optimal volume of R134a as the working fluid is 50% relative to the volume of the evaporator. Park et al. [25] studied a TPLTS with FC-72 as the working fluid, and concluded that a 10% fill ratio resulted in dry-out, and a 50% fill ratio resulted in flooding, therefore the optimal fill ratio is between those two values. Fu et al. [13] reported the fill ratio should be between 30 and 80% of the total loop volume with ammonia as the working fluid. Values less than 30% resulted in dry-out and values greater than 80% resulted in flooding. Beitelmal & Patel [1] report optimal charge amounts to be between 10% and 15% PF-5060 relative to the total volume available in the evaporation chamber. Based on the literature review discussed above, it is clear the optimal fill ratio varies greatly depending on the working fluid and other system parameters, including size of the evaporator relative to the remainder of the loop.

The third type of thermosyphon is the single-phase loop thermosyphon (SPLTS) which is also sometimes referred to as single-phase natural circulation loop, a general schematic of which is shown in Fig. 1d. The basic structure is the same as that of a TPLTS where there is an evaporator section that heats the working fluid, a pipe connects the evaporator to the condenser (riser), the condenser cools the working fluid, and another pipe connects the condenser to the evaporator (downcomer) through which the working fluid flows back to the evaporator. The flow is driven by the hydrostatic pressure difference that results from the temperature gradient and resulting density gradient from the evaporator to the condenser. Fluid motion is generated by density differences in the due to temperature gradients generated by the evaporator and condenser [20]. The motion is governed by the balance of the opposite effects of buoyancy (due to the different fluid densities in the ascending (warm) and descending (cold) sections), and friction [21]. Generally, the heat sink is above the heat source to enhance the circulation rates [32]. A disadvantage of the SPLTS is that interaction between buoyancy and frictional forces can be unstable. There is also an expansion tank shown in Fig. 1d which may be present in a SPLTS to accommodate the volume expiation of working fluid as temperature increases.

The single-phase LTS studied by Dobson & Ruppersberg [6] also has an expansion tank into which excess fluid flows as a result of thermal expansion. The expansion tank serves to ensure the pressure in the loop does not get too high. Pilkhwal et al. [26] also used an expansion tank in their experiment to allow for the expansion of working fluid (in this case water). Naveen et al. [24] explain the expansion tank is necessary to vent the air out during the loop filling, and to accommodate the swells and shrinkages of the fluid within the loop during transient operation. Typically, the SPLTS is fully filled with liquid working fluid.

The NPCHP was proposed by Lee et al. [17,18] as a new heat pipe. They report the phase change of the working fluid is suppressed at steady state operation, and the heat transfer is dependent on the pressure increase from the temperature increase of the working fluid, rather than phase change, as in conventional heat pipes. Since the NPCHP does not rely on phase change, a wick is not necessary. Preliminary results on the operation of the NPCHP identify heat transfer modes [17,18]. Their efforts also focused on the qualitative performance of the NPCHP, but lacked detailed quantitative results. Our focus is to show, through quantitative experimental and numerical results for various fill ratio and heat input parameters, the NPCHP is not a new heat pipe but instead operates as either a single- or two-phase loop thermosyphon based on working fluid and liquid fill ratio and is subject to the corresponding limitations.

2. Experiment setup

The NPCHP experiment consists of a loop of stainless-steel pipe filled with R134a as the working fluid. R134a was chosen as the working fluid due to its compatibility with stainless steel and because the thermosyphon can operate at room temperature. A diagram of the experiment is shown in Fig. 2. The evaporator section (1), consists of three AC 110 V 100–300 W 2 Wire Mold Cartridge Heater Pipe Heating Elements (12 mm × 80 mm). A pressure release valve (2) is added to release pressure from the system if it increases above 350 psi. Fluid release and fill valves (3) are used to add and remove working fluid from the system. The condenser section of the NPCHP consists of a cooling jacket (4) surrounding a section of the pipe. Cold water (~5 °C), which is cooled by two LAUDA Alpha RA8 water coolers (5), flows through the cooling jacket. Heat is transferred out of the system into the cooling water. The flowmeter (FL-3440ST) (6) is used to adjust the flow rate of the cooling water moving through the cooling jacket. The variable automatic transformer (Staco Energy Products Co 3PN1510) (7) adjusts the power supplied to the heating element. The digital wattmeter (Vector-Vid WD-767) (8) reads the value of power supplied to the heating element.

The pipe material is stainless steel with outer and inner diameters of 12.7 mm and 10.9 mm, respectively. The pipe is almost entirely filled with liquid R134a, a typical fill amount is 90–95% relative to total loop volume. The overall height and width of the pipe are 1.465 m and 0.395 m, respectively. The pipe is oriented vertically with the heating element below the condenser on opposite sides of the pipe. The entire pipe is insulated with 1 in. thick ceramic fiber insulation. The heating element is surrounded by three layers of insulation.

K-type thermocouples and pressure transducers (Digi-Key P51-500-A-A-I36-5 V-000-000 500 Psia 1/4NPT 5 V) are placed at multiple locations around the loop. Instrumentation locations are shown in Fig. 2. Thermal response time of the system to a heat input can be observed by plotting temperatures at various locations with time.

The pressure transducers are used in concurrence with the temperature at those locations to determine the phase of the working fluid with time and location around the loop. Since the main driver for heat transfer in the NPCHP is the pressure response to the heat input, it is important to understand how the pressure changes throughout the experiment.

Thermocouples T1-5, T10, T11, and T14 are placed on the outside of the pipe. T10 measures the temperature just before the evaporator, T5 measures the temperature just after the evaporator, T4 measures the top center (TC) temperature, T2 and T11 are the temperatures before and after the condenser, respectively, and T1 is the bottom center (BC) temperature. T8-9 and T6-7 are the cooling water inlet and outlet temperatures, respectively. T12 measures the temperature of the working fluid inside the pipe. T13 measures the temperature of the heating element.

3. Numerical simulation

The multi-fluid model is one method for the formulation of macroscopic equations of a multiphase system, obtained using phase averaging. The multi-fluid model performs averaging for each individual phase within a multiphase control volume [11]. In this computational model, one set of equations is generated for each phase present in the system. These equations describe the flow

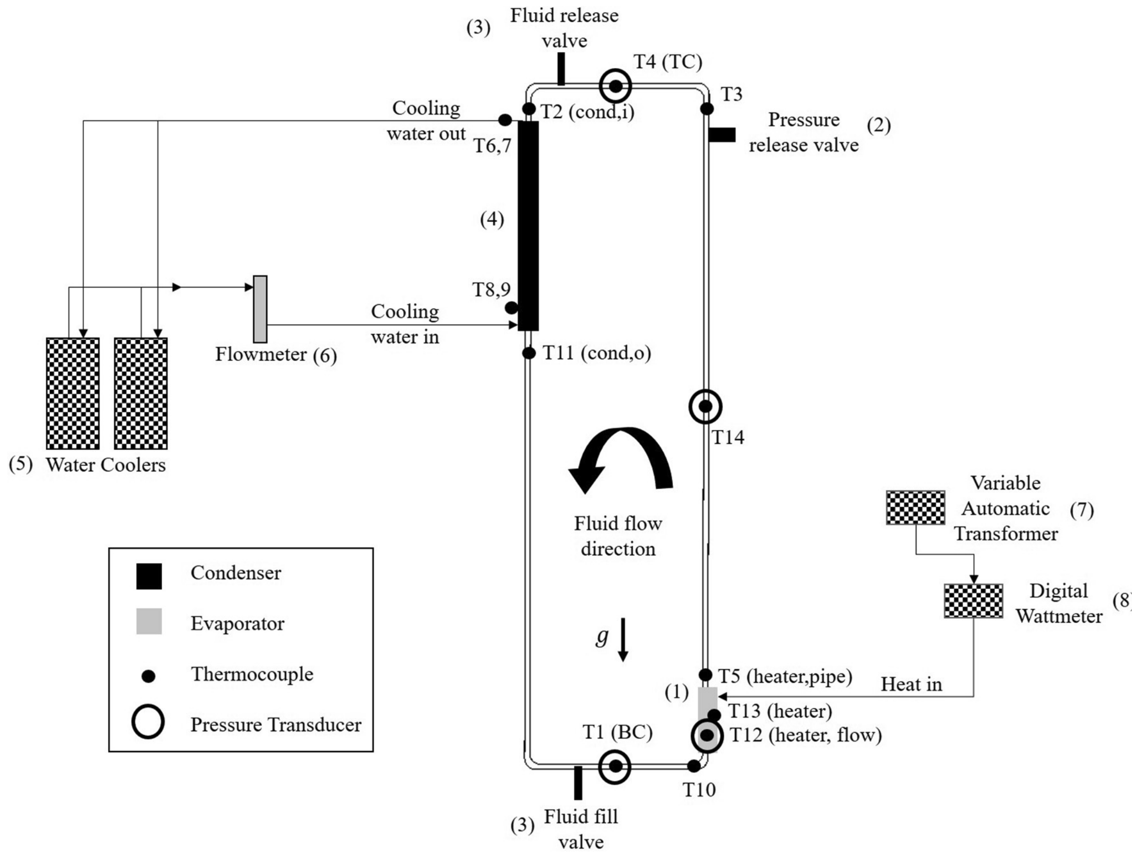

Fig. 2. Layout of the NPCHP Experimental Setup Showing Thermocouple and Pressure Transducer Locations.

within the control volume. The mixture model is another method for the formulation of macroscopic equations of a multiphase system. In the mixture model, spatial averaging is performed over both phases simultaneously within the control volume, and the phases are considered together as a whole [11]. Governing equations for the mixture model are obtained by adding the multi-fluid equations for each phase. Therefore, only one equation is solved for each conservation equation. The mixture model solves the momentum equation by describing the dispersed phases with relative velocities. The Ansys FLUENT VOF model [33] is used to model multiphase flow in the NPCHP and uses both multi-fluid and mixture models to describe the flow for this 2D transient model.

In this approach, the multi-fluid model is used to solve the continuity equation; there is one equation for each phase present in the multiphase control volume. The following equation describes the continuity equation for the volume fraction of each phase to track the interface between phases [11]:

$$\frac{\partial}{\partial t}\left(\varepsilon_k\langle\rho_k\rangle^k\right)+\nabla\cdot\left(\varepsilon_k\langle\rho_k\rangle^k\langle\mathbf{V}_k\rangle^k\right)=\sum_{j=1(j\neq k)}^{\Pi}\left(\dot{m}_{jk}'''\right) \tag{1}$$

Since the sum of the volume fraction of all the fluid phases present in each computational cell must sum to 1, volume fraction is solved for each phase except the primary phase, which is defined based by ease of modeling to be the liquid phase working fluid. The volume fraction of the primary phase is determined by solving for the volume fraction such that the sum of all volume fractions is 1.

The mixture model is used to solve the momentum equation. A single momentum equation is solved throughout the domain, which is dependent on the volume fractions of all the phases. The properties in the momentum equation are calculated based on the phases in each control volume. The mixture model momentum equation is:

$$\frac{\partial}{\partial t}\left(\langle\rho\rangle\widetilde{\mathbf{V}}\right)+\nabla\cdot\sum_{k=1}^{\Pi}\varepsilon_k\langle\rho_k\rangle^k\langle\mathbf{V}_k\mathbf{V}_k\rangle^k=\nabla\cdot\langle\boldsymbol{\tau}\prime\rangle+\langle\rho\rangle\mathbf{X}+\dot{\mathbf{M}}_I''' \tag{2}$$

The energy equation, like the momentum equation, is shared among the phases and uses the mixture model. The mixture model energy equation is [11]:

$$\frac{\partial}{\partial t}\left(\langle\rho\rangle\widetilde{h}\right)+\nabla\cdot\left(\sum_{k=1}^{\Pi}\varepsilon_k\langle\rho_k\rangle^k\langle\mathbf{V}_kh_k\rangle^k\right)$$
$$=-\nabla\cdot\langle\mathbf{q}''\rangle+\frac{D\langle p\rangle}{Dt}+\langle q'''\rangle+\nabla\widetilde{\mathbf{V}}:\langle\boldsymbol{\tau}\rangle+q_{\boldsymbol{I}}''' \tag{3}$$

Assumptions and boundary conditions are applied to the model as follows: there is a heating section around part of the outside of the pipe modeled as constant heat flux, and a cooling section around another section modeled as convection heat transfer, the remainder is modeled as adiabatic.

The pressure-based, transient, planar solver is used. Pressure-based methods are used for incompressible and low Mach number flows, whereas the density-based solver is used for transonic and supersonic flow fields [28]. Since the flow through the pipe is not high speed, the pressure-based solver is appropriate, and the explicit scheme is used. Sharp/dispersed is used for the interface modeling. The sharp model is applicable when there is a distinct interface between the two phases, dispersed is used when the phases are interpenetrating, and sharp/dispersed is a combination of the two (Choosing Volume Fraction Formulation). The energy equation is used to model the phase change of liquid to vapor working fluid, and vice versa. The flow is modeled as laminar, and the SIMPLE algorithm for pressure-velocity coupling is used.

The saturation temperature for R134a is defined as a function of saturation pressure. The saturation temperature (K) and pressure (Pa) are related using a polynomial relationship: $T_{sat} = -1.12\times 10^{-23}P^4 + +5.71\times 10^{-17}P^3 - 1.16\times 10^{-10}P^2 - 1.43\times 10^{-4}P + 239.96$ obtained for a pressure range of approximately 2.9–16.8 bar, which is within the operational range of the experiment [30]. If the simulation pressure increases beyond this range, the polynomial relationship will be followed until the simulation maximum pressure limit of 500,000 bar is reached and the simulation will output an error and stop running. There is a mass interaction between liquid R134a and R134a vapor in the initial startup phase of the NPCHP, where the interaction mechanism is evaporation-condensation. Evaporation-condensation is modeled using the Lee Model [19]. The Lee model uses the following equations to calculate mass transfers:

$$\dot{m}_v = -\dot{m}_l = r\varepsilon_l\rho_l\frac{T - T_{sat}}{T_{sat}} \quad T > T_{sat}(\text{evaporation process}) \tag{4}$$

$$\dot{m}_l = -\dot{m}_v = r\varepsilon_v\rho_v\frac{T_{sat} - T}{T_{sat}} \quad T < T_{sat}(\text{condensation process}) \tag{5}$$

According to [38], the value of r is recommended to be such as to maintain the interfacial temperature reasonably close to the saturation temperature, and to avoid divergence issues.

The system is divided into regions where each region is specified with initial conditions; a small fraction of the volume, usually 5–10%, is specified to have an R134a vapor volume fraction of 1, the remainder is saturated liquid R134a. The region surrounded by the cooling jacket has an initial temperature of 288 K. These initial conditions are chosen based on the physical experiment. The temperature of R134a in the loop at the location surrounded by the cooling jacket is initially colder than the rest of the loop, and is therefore set with a lower initial temperature of 288 K.

A grid independence study was performed to ensure the numerical simulation is independent of the mesh size. Fig. 3 plots the temperature of the top center (TC) and bottom center (BC) of the loop from 0 to 1000 s for two different mesh. Data series "TC" and "BC" are temperature readings from the 40,909-element mesh. For data series "TC fine" and "BC fine", the max face size of the mesh was decreased to 0.5 mm instead of 1.0 mm, which resulted in 171,304 elements (approximately 4 times as many as original mesh). Mesh quality data is shown in Table 1.

For the first 400 s, the temperatures are very close between the two meshes at the TC location, and for the first 500 s at the BC location. At the TC, the temperature readings after 400 s are slightly different between the two meshes, but the average steady state temperature is the same. After 500 s, the temperature readings at the BC are slightly different between the two meshes. The temperature at the BC of the fine mesh increases slower than that of the initial mesh, but by 900 s reaches the same average steady state temperature as the initial mesh. Since the average steady state temperature at each location for the two different meshes are very close, and the paths are similar, the grids are independent. Table 2 shows the average steady state temperature for the two meshes at each location. Since the percent difference between the two meshes is less than 1%, and the computational time increases to 4 days, the increased computational time is not justified, and the initial grid sizing is used.

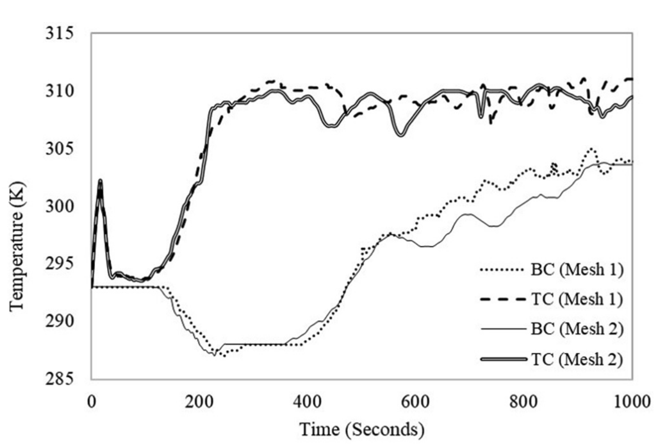

Fig. 3. Grid Independence Study on Temperature Distribution at Locations TC and BC for the Numerical Simulation of NPCHP.

Table 1
Mesh Quality, Initial and Fine Meshes for Numerical Simulation of NPCHP.

	Initial Mesh (Mesh 1)	Fine Mesh (Mesh 2)
Max Face Size (mm)	1.0	0.5
Total Elements	40,909	171,304 (300% ↑)
Min Orthogonal Quality	0.63	0.65 (3% ↑)
Max Aspect Ratio	7.14	4.65 (35% ↓)
Computational Time (using 7 cores)	~1 Day	~4 Days

Table 2
Mesh Convergence Study Steady State Temperature at TC and BC Locations for Two Meshes used in NPCHP Numerical Simulation.

Mesh Elements	TC Steady State Temperature (K)	BC Steady State Temperature (K)
40,909	309.75	303.76
171,304	309.43	303.62
Percent Difference	0.87%	0.46%

In this case, the initial fill ratio is 95% liquid, the heat input is 200 W, and the convection coefficient at the condenser is 112 W/m^{2}K. The convection coefficient was calculated based on the theoretical amount of heat that is output through the condenser, and the condenser surface area. Fig. 4 shows the temperature at four locations around the loop for the simulation and experiment.

Steady state temperatures are important because they are used in many of the analysis methods (for finding temperature drop and thermal conductivity). Fig. 4 shows the temperature response is similar between the simulation and experiment. Table 3 lists the steady state temperatures at four locations around the loop for 200 W, 250 W, and 300 W heat inputs.

While there are fluctuations in the data, it can be seen from Table 3 the maximum percent difference between steady state temperatures of the experiment and simulation is 2.51% for all the cases shown in Table 3. The experimental uncertainty associated with each temperature reading is 0.42 K. The simulation values generally do not fall within this uncertainty but the simulation is still able to predict steady state temperature reasonably well given the assumptions made during modeling

4. NPCHP exhibits characteristics of a loop thermosyphon

There are several characteristics that classify heat transfer devices as heat pipes, with loop thermosyphons being a type of heat pipe where the flow of working fluid is driven by gravity and no wick structure is required. A heat pipe has a high effective thermal conductivity, which means it can transfer the same amount of heat, with a much smaller temperature difference between the evaporator and condenser, than a solid metal rod of

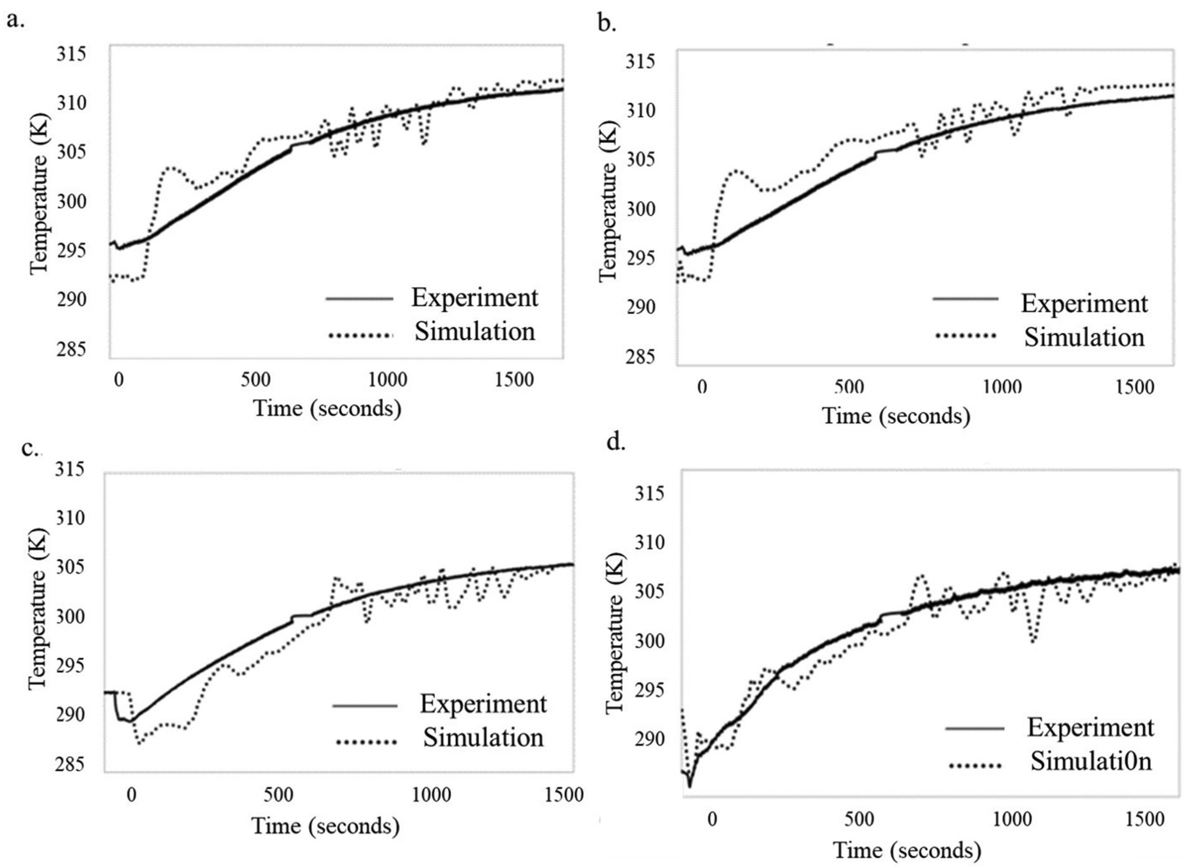

Fig. 4. Comparison of Temperature Response in the NPCHP Numerical Simulation to the NPCHP Experiment with 200 W Heat Input and 90% Fill Ratio at Four Locations: (a). Before Condenser (T2), (b). TC (T4), (c). BC (T1), (d). After Condenser (T11).

Table 3
Steady State Temperature Comparison Between Numerical Simulation and NPCHP Experiment with 200 W, 250 W, and 300 W Heat Inputs.

Heat Input (W)	Steady State Temperature	T2 (K)	T4 (K)	T1 (K)	T11 (K)
200	Simulation	311.60	311.79	306.07	305.56
	Experiment	307.77	307.21	305.67	303.15
	Percent Difference	1.23%	1.47%	0.13%	0.79%
250	Simulation	311.97	312.00	308.51	307.41
	Experiment	313.42	313.10	310.72	307.77
	Percent Difference	0.46%	0.35%	0.72%	0.12%
300	Simulation	313.73	313.98	306.48	308.85
	Experiment	315.90	315.72	314.16	311.32
	Percent Difference	0.69%	0.55%	3.51%	0.80%

comparable size [9]. A heat pipe can transport large quantities of heat rapidly through a small cross-sectional area over a considerable distance with no additional power input to the system and can take in energy through a small surface area and transfer the same amount of energy out over a larger surface area. The ratio of thermal flux, the heat flux into the evaporator divided by the heat flux out through the condenser, is called the thermal flux transformation ratio and can be as large as 15 to 1 [9]. We will demonstrate, through experimentation and numerical simulation, that the NPCHP exhibits the following characteristics:

1. High effective thermal conductivity
2. High heat transport capability
3. Fast thermal response time
4. High heat flux transformation ratio
5. High heat flux

4.1. High effective thermal conductivity

A heat pipe has a high effective thermal conductivity, which means it can transfer the same amount of heat, with a much smaller temperature difference between the evaporator and condenser, than a solid metal rod of comparable size.

The effective thermal conductivity k_{eff}, is the thermal conductivity a rod with the same diameter as the heat pipe would need to transfer the same amount of heat over the effective length L_{eff}:

$$L_{eff} = \frac{L_e}{2} + L_a + \frac{L_c}{2} \tag{6}$$

$$k_{eff} = \frac{L_{eff}\dot{Q}_{in}}{(T_{e,ave} - T_{c,ave})A_c} \tag{7}$$

Based on experimental data, the nominal effective thermal conductivity is on the order of 10^6 W/m K. This means that a metal rod of similar size would need a thermal conductivity on the order of 10^6 W/m K to transfer the same amount of heat as a NPCHP. Fig. 5 shows the average steady state effective thermal conductivities for heat inputs ranging from 200 W to 300 W, in 50 W increments for the numerical simulation and experiment. Error bars are added corresponding to the standard deviation of the experimental values. The highest effective thermal conductivity occurs for the highest heat input, which indicates the resistance to the flow of heat decreases with increasing heat input, and the device operates most effectively for the 300 W heat input.

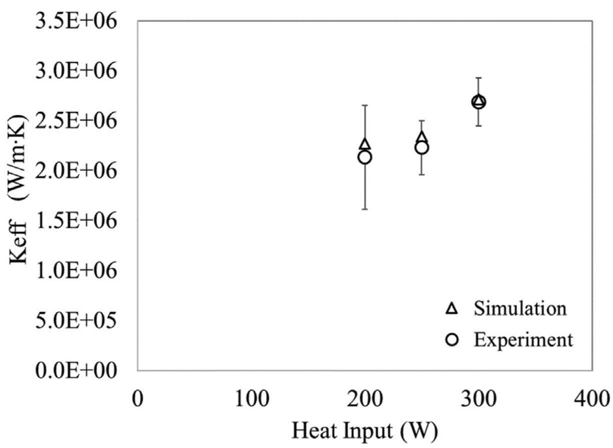

Fig. 5. Steady State Effective Thermal Conductivity of NPCHP with 90% R134a Fill Ratio for Experiment and Simulation with Heat Inputs of 200 W, 250 W, and 300 W.

For comparison, the thermal conductivity of copper, which is a relatively high thermal conductivity metal, is 400 W/m K. The experimental effective thermal conductivity for a 200 W heat input is over 6000 times larger than that of copper. This shows that the requirement for a heat pipe to have a high effective thermal conductivity is met by the NPCHP.

4.2. High heat transport capability

In this experiment, heat travels approximately 1.8 m through a 9.37×10^{-5} m^2 cross-sectional area pipe before reaching the cooling jacket. Therefore, the NPCHP transports large quantities of heat through a small cross-sectional area over a considerable distance with no additional power input to the system.

Fig. 6 shows the temperature response of the NPCHP measured at four different locations around the system to a heat input applied at the evaporator section. As seen in Fig. 6, the NPCHP reaches steady state for each of the three heat inputs shown, which means it is capable of transporting between 200 and 300 W from the evaporator section to the condenser section. It can also be seen that the overall temperature is lower for lower heat inputs.

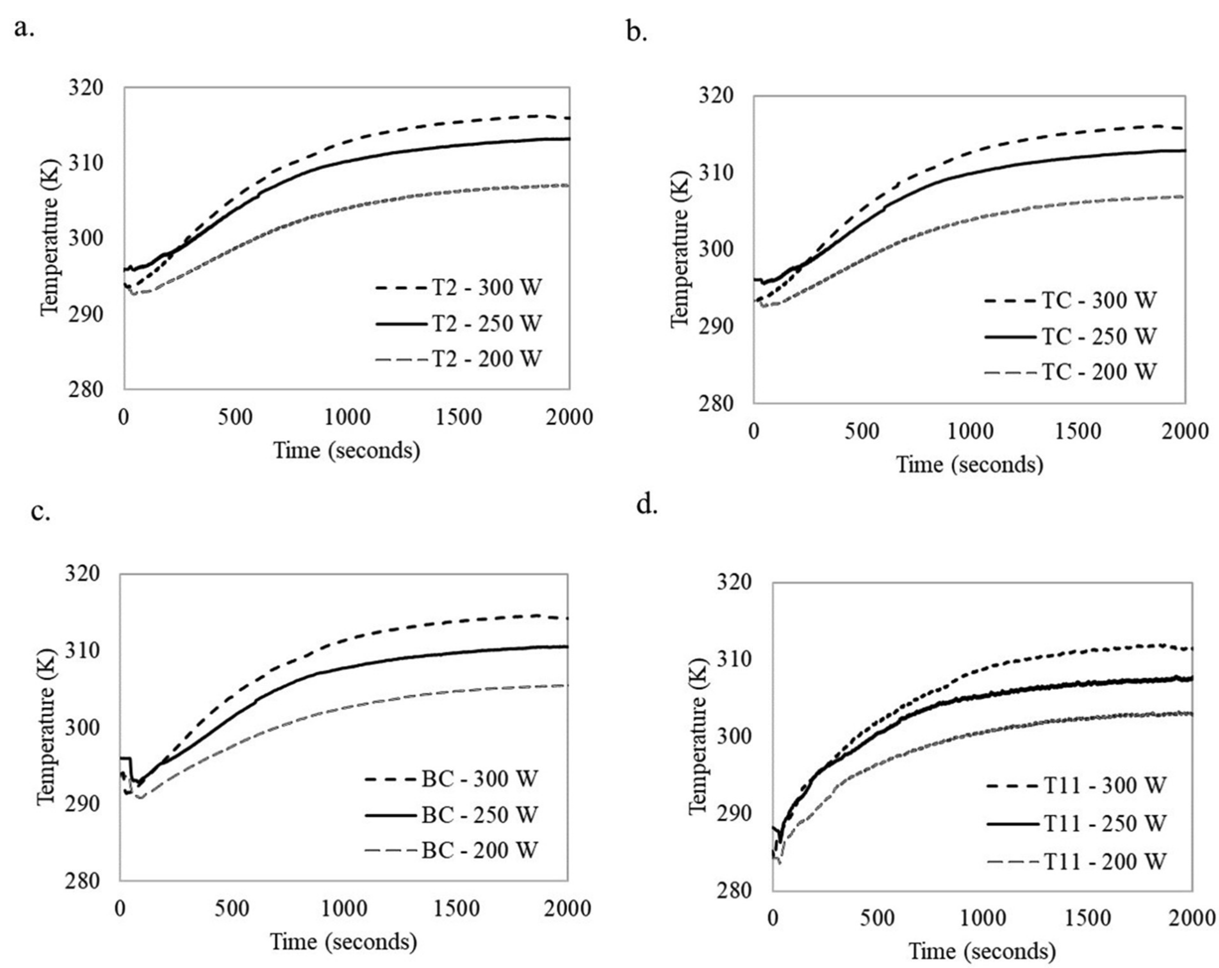

Fig. 6. Comparison of NPCHP Experiment Thermal Response Time for Heat Inputs of 200–300 W with 90% R134a Fill Ratio at (**a**). Cond(i), (**b**). TC (T4), (**c**). BC (T1), (**d**). Cond (o).

The temperature drop between the evaporator and condenser section is an important characteristic to note, as one characteristic of a heat pipe is a small temperature drop between the heat source and the heat sink. Under steady state operation, heat is added to the evaporator at an average evaporator temperature, and the same quantity of heat is rejected at a lower average condenser temperature.

The temperature drop is calculated as the difference between the average evaporator temperature and the average condenser temperature. Fig. 7 shows the steady state temperature drop between the evaporator and condenser sections of the NPCHP. Steady state temperature drops are plotted for experiments and simulations with 200 W, 250 W, and 300 W inputs and a 90% initial liquid fill ratio. Error bars are added corresponding to the standard deviation of the values obtained from the experiment. The steady state temperature drop increases slightly from the 200 W heat input experiment to the 250 W and 300 W heat input experiments.

The temperature drop obtained from the numerical simulation follows the same trend as the experiment and fall within the error range from the experimental values.

4.3. Fast thermal response time

Thermal response time of a heat pipe is how fast the system responds to a heat input. Heat pipe thermal response time is based on the variation of heat pipe surface temperature in a transient analysis [29]. Fig. 8 shows the thermal response of the NPCHP experiment to an applied heat input of 200 W. The heat input is applied at t = 0 s. The temperature around the loop begins to increase almost immediately, and increases steadily for the first 1000 s, when the temperatures begin approaching a steady value. This shows that the NPCHP experiment has a very fast thermal response time, as the temperatures change in response to the heat input almost immediately after the heat input is applied. The system reaches steady state operating conditions (temperature is no longer changing with time) after 2500 s for a heat input of 200 W.

The thermal response time of the NPCHP can be compared to a copper rod to determine if the NPCHP is an effective heat transfer device and show the speed at which the heat is transferred through the system. A numerical simulation was created to model heat transfer through a copper rod. The rod is modeled as 2D with the same diameter as the NPCHP experiment, and length of 2 m, similar to the adiabatic length of the NPCHP (the distance between the heater and the cooling jacket, which is 1.8 m). The temperature before the condenser inlet is used to compare the thermal response time of a copper rod because it is the farthest point on the adiabatic section of the pipe before the cooling jacket. Even though copper is a high thermal conductivity metal, it is expected that the temperature of the NPCHP at 2 m from the heat source increases much faster than a point an equal distance from the heat source on the copper rod. This is because the effective thermal conductivity of a heat pipe is much larger than the thermal conductivity of metals, including copper. The heat is expected to be able to travel much faster and with less resistance through the NPCHP than copper rod.

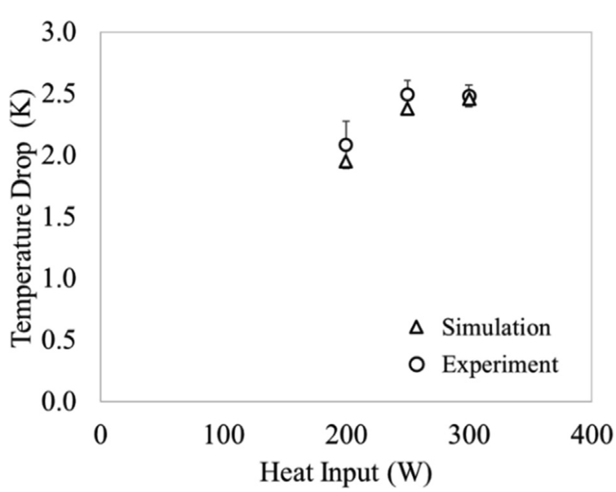

Fig. 7. Steady State Temperature Drop of NPCHP Experiment and Simulation with 90% R134a Fill Ratio for Heat Inputs of 200 W, 250 W, and 300 W.

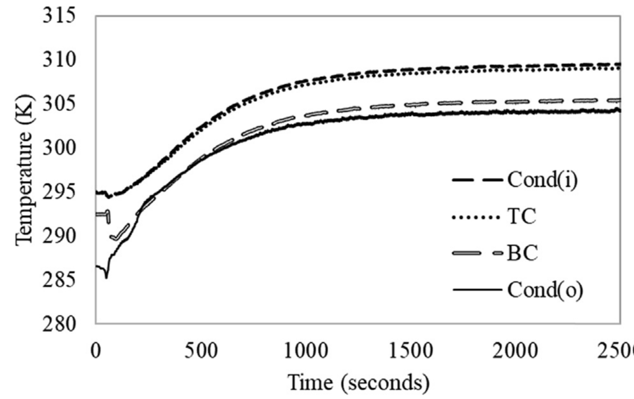

Fig. 8. Thermal Response Time of NPCHP Experiment with 90% R134a Fill in Response to 200 W Heat Input.

The temperatures obtained from the copper rod simulation are recorded at 2 m from the heater and compared to the temperature before the condenser inlet of the NPCHP experiment. Fig. 9 shows the copper rod simulation geometry.

Fig. 10 shows the temperature at the condenser inlet (T2) increases much faster than the temperature 2 m from the heat source on a copper rod, which increases about 1 K in the 2000 s the simulation was run.

The thermal response time of the NPCHP is much faster than that of the copper rod for a point at the same distance from the heat source, which is the expected result. Therefore, the NPCHP is capable of transferring heat much more rapidly than a comparably sized rod made of a high thermal conductivity metal.

4.4. High heat flux transformation ratio

Another characteristic of a heat pipe is that it can take in energy from a small surface area and transfer that energy out over a large surface area. The ratio of heat flux, which is the heat flux into the evaporator divided by the heat flux out through the condenser, is called the thermal flux transformation ratio and can be as large as 15 to 1. In the NPCHP experiment, thermal flux transformation ratio is calculated to be approximately 11. Therefore, the NPCHP experiment takes in energy through a small surface area and transfers energy out through a large surface area, thus exhibiting another characteristic of a heat pipe.

The heat transfer in a NPCHP can be described by a cycle as follows: there is a heat input to the evaporator section, a relatively constant working fluid temperature between the evaporator and condenser, a heat output from the condenser section, and a relatively constant working fluid temperature between the condenser and evaporator. This cycle is shown in Fig. 11.

The relatively constant temperature between the evaporator and condenser section (in either direction) can be shown experimentally and from the simulation. Fig. 12 shows the steady state temperature at different locations around the loop for three different heat inputs (200 W, 250 W, and 300 W) for a 90% R134a liquid

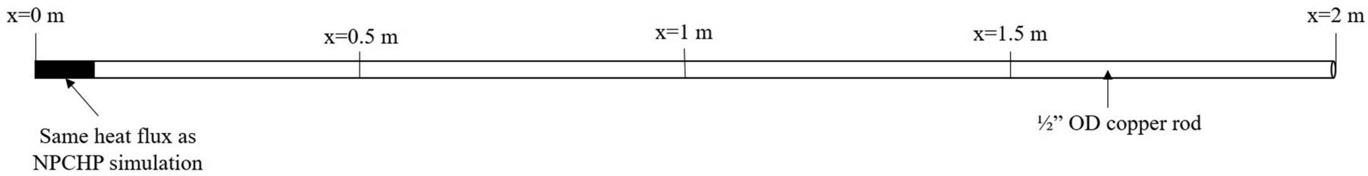

Fig. 9. Copper Rod Numerical Simulation Geometry for Comparison with NPCHP Experiment Thermal Response.

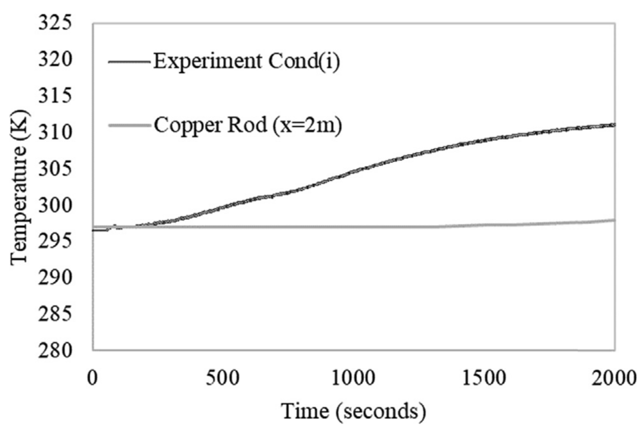

Fig. 10. Thermal Response Time of Copper Rod Simulation Compared to NPCHP Experiment with 90% R134a Fill Ratio and 200 W Heat Input at the Condenser Inlet.

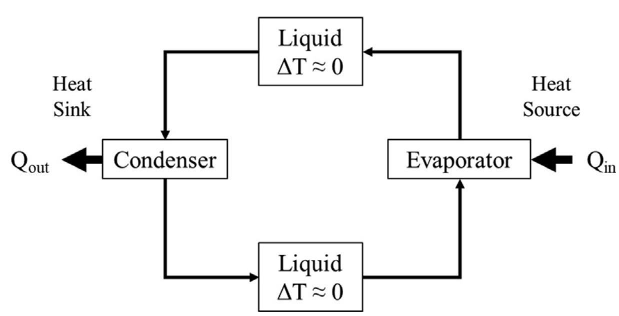

Fig. 11. Thermodynamic Cycle of the NPCHP at Steady State Operating Conditions After Initial Startup Period.

fill ratio. As seen in Fig. 12, the temperature of the working fluid from the evaporator to condenser is near constant with maximum fluctuations of 0.3 K for the experiment and 1.2 K for the numerical simulation. There are larger fluctuations in temperature from the condenser to the evaporator with a maximum temperature difference of 1.5 K for both the experiment and numerical model.

This data shows that the NPCHP can take in energy through a small surface area (evaporator) and transfer the energy out over a larger surface area (condenser).

4.5. High heat flux

Another characteristic of a heat pipe is a high heat flux, which is the amount of heat transferred per unit area. Maximum radial heat flux at the evaporator, the maximum heat transferred into the heat pipe per unit surface area of the evaporator, is calculated using [34]:

$$q_{r,max} = \frac{\dot{Q}_{max}}{A_s} \tag{8}$$

The heat flux into the evaporator is compared to the heat flux out through the condenser to determine the heat flux transformation ratio. The maximum heat flux measured in the experiment is 230,361 W/m^2. This value was compared to data from existing heat transfer devices [9] based on the effective length of the heat pipe. Results are shown in Fig. 13.

While there is scatter in the results shown in Fig. 13, the data point for the NPCHP lies well above the remainder of the data. This shows that the heat flux in the NPCHP is greater than that of existing heat transfer devices when analyzed as a function of heat pipe effective length. The NPCHP therefore can be said to have a high heat flux and exhibits another characteristic of a heat pipe.

5. Effect of fill ratio

The experiment has been tested with fill ratios ranging from 25% to 99%. The working fluid used in all the experiments is R134a. After running the experiment with fill ratios of 25–99% relative to the total volume of the pipe while removing working fluid in increments of approximately 5% between experiments, it was determined that the 99% fill ratio experiment is not able to reach steady state at a heat input of 200 W. The maximum heat input at which each fill ratio experiment was able to reach steady state is listed in Table 4. Based on these results, the experiments with fill ratios of 70–75% can transfer the most heat.

The pressure changes within the system in response to a heat input with varying fill ratios corresponding to the previously mentioned experiments were studied. For the experiments discussed below, the pressures at the TC and BC location were plotted. Each plot also contains the saturation pressure corresponding to the temperature recorded at the given location. The pressure results for the 95% fill ratio experiment are shown in Fig. 14. The 99% and 95% fill ratio experiment are the only experiments where the system reached the fully filled condition and became single phase. The fully filled condition is defined as the condition when the working fluid within the loop expands to fill the entire volume, and volume expansion is limited. This was determined by the large spike in pressure, as shown in Fig. 14 for the 95% experiment, which indicates when volume expansion is limited, since any increase in temperature after the working fluid expands to fill the pipe results in a significant increase in pressure. The 95% experiment reached steady state at 200 W. Then, the heat input was increased in increments of 10 W, and allowed to reach steady state, until 260 W when the pressure began to rise steeply. At this point, the heating element was shut off, as indicated by the "0W" label on Fig. 14.

It can be seen in Fig. 14a that the pressure, after about 8000 s, begins to rise above the saturation pressure at the TC (T4) location. This indicates the working fluid is in the compressed liquid phase, rather than a saturated vapor or liquid-vapor mix. When the filly filled state is reached, volume expansion is limited. Therefore, any additional increase in temperature is accompanied by a rapid rise in pressure, as shown in Fig. 14. Fig. 14b shows the saturation pressure and system pressure at the BC location. The system pressure is always greater than the saturation pressure, indicating the working fluid is always a compressed liquid at the BC location. The 99% fill ratio experiment exhibited similar characteristics with a steep pressure rise occurring before the system was able to reach steady state for a 200 W heat input. This indicates the 99% fill ratio

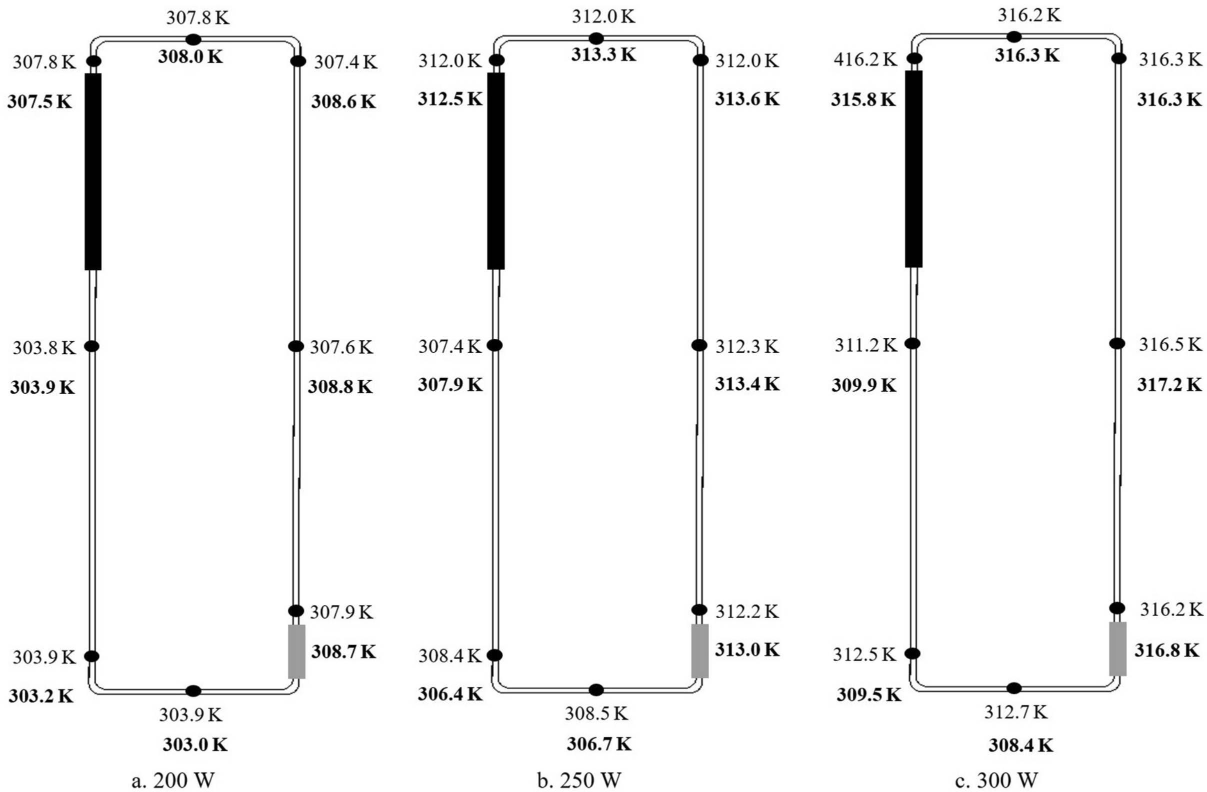

Fig. 12. Steady State Temperatures Around NPCHP Experiment and Numerical Simulation (bolded) for Heat Inputs of (a). 200 W, (b). 250 W, (c). 300 W.

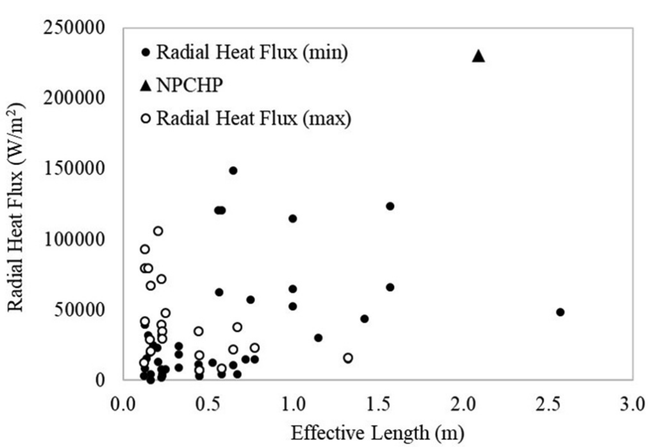

Fig. 13. Heat Pipe Heat Flux as a Function of Effective Length Compared Between NPCHP and Experimental Data for Other Heat Transfer Devices*. *Note: This includes different types of heat pipes, heat pipes made from various materials, and using different working fluids.

Table 4
Maximum Heat Input at which Each Fill Ratio Experiment Can Reach Steady State with R134a as Working Fluid.

Fill Ratio (% relative to total loop volume)	Maximum Heat Input at which Steady State is Reached
99%	Not able to reach steady state at 200 W heat input
95%	200 W
90%	300 W
85%	300 W
80%	300 W
75%	325 W
70%	325 W
65%	300 W
60%	300 W
55%	300 W
50%	300 W
45%	300 W
40%	300 W
35%	300 W
30%	250 W
25%	Not able to reach steady state at 200 W heat input

experiment reaches the fully filled condition earlier, as expected. The 99% and 95% experiments operate as TPLTS until the system becomes fully filled and is no longer able to operate due to the significant pressure rise.

The pressures at the flow/heater and BC locations are plotted for the 55% fill ratio experiment in Fig. 15 at the heater/flow and BC locations. As seen in Fig. 15a, the saturation pressure is equal to or slightly greater than the system pressure at the heater/flow location. This indicates the working fluid is vapor or liquid vapor mix just after the heater. However, at the BC location shown in Fig. 15b, the system pressure is greater than the saturation pressure, indicating that the working fluid at the BC of the loop is a liquid. With lower fill ratios, including the 55% fill ratio, the NPCHP operates as a TPLTS.

Based on experimental data, the experiments with fill ratios of 95–99% reach single phase since the system pressure is greater than the saturation pressure at all locations when a high enough heat input is applied (250 W for the 95% fill ratio experiment and 200 W for the 99% experiment). The experiments with fill ratios less than 95% are two-phase. The system pressures for these fill ratio experiments at the heater location are less than or equal to the saturation pressure, indicating vapor or liquid-vapor mix, and the system pressure at the BC location is greater than the saturation pressure meaning the working fluid is a compressed liquid.

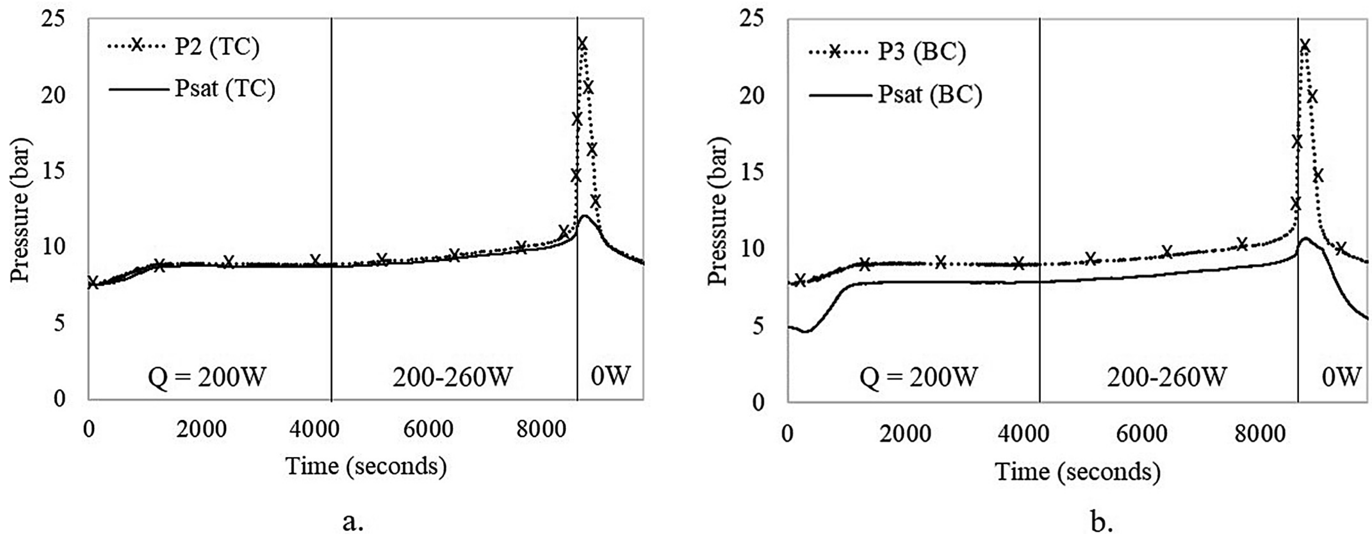

Fig. 14. Pressure Response to Heat Input at (a). TC (T4), (b). BC (T1) for 95% R134a Fill Ratio and Heat Inputs from 200 to 260 W.

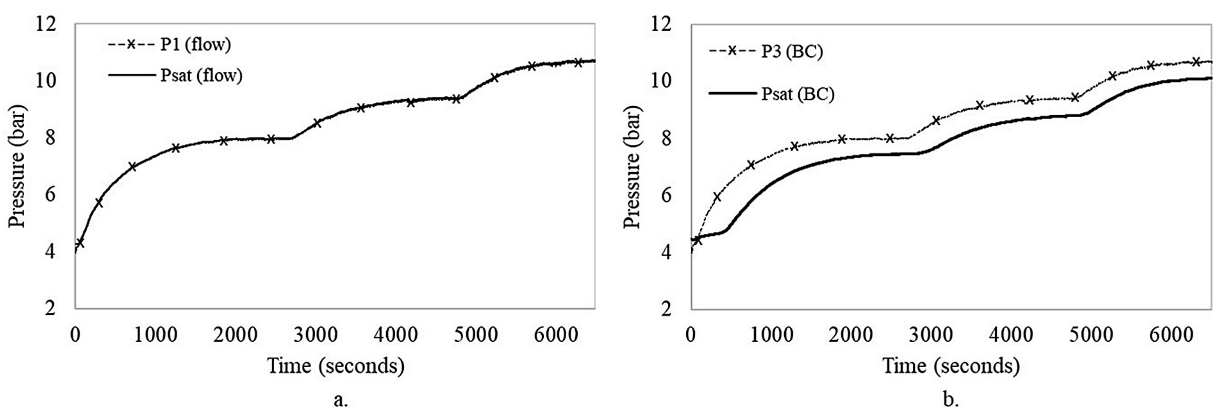

Fig. 15. Experimental Pressure Data of 55% R134a Fill Ratio with Heat Inputs of 200–300 W at a. the location of the Flow and b. at the BC location.

Therefore, the only experiments where the phase change is inhibited are the 95–99% experiments when sufficient heat is applied to the system.

These experimental results agree with theoretical predictions based on volume expansion and initial experimental conditions. The NPCHP is initially filled with a predetermined amount of working fluid. As the temperature of the working fluid increases, it expands to fill the entire pipe (if the initial fill ratio and heat input are high enough). According to Lee et al. [17,18] the working medium inside the NPCHP comes to a fully filled state under a certain heating condition. In this state, the volume expansion and the phase change of the working medium in the pipe caused by temperature rise is restrained. Table 5 shows the volume expansion coefficients corresponding to the specific temperature and pressure of each experiment that was run ranging from 80 to 95% fill ratios. The temperature change required to fill the entire pipe is calculated and added to the initial temperature of the working fluid to determine the temperature the working fluid inside the experiment must reach to fully fill the pipe.

The R134a within the loop should remain below 50 °C (323 K), as required by the safety data sheet. This means that the fully filled state can be reached for fill ratios of 95% or greater, which agrees with the experimental results obtained by comparing saturation and system pressures discussed previously.

Table 5
Volume Expansion Coefficients and Temperature Increase Required to Reach Fully-Filled State.

Fill Ratio	α (1/K)	$T_{initial}$ (K)	ΔT (K)	T_{final} (K)
95%	3.670×10^{-3}	292.71	14.34	307.05
85%	4.683×10^{-3}	290.40	37.69	328.09
80%	4.589×10^{-3}	289.22	54.48	343.70

6. NPCHP working mechanisms

The following analysis is presented for a NPCHP where the fill ratio is high enough that the system reaches the fully filled state. This fill ratio was determined to be 95% or greater for R134a as the working fluid, depending on the heat input. Pressure transducer locations are shown in Fig. 2. A graph of the pressure response is shown in Fig. 14 for an initial fill ratio of 95%. For fill ratios greater than or equal to 95%, but less than 100%, the working fluid is initially two-phase. Fig. 14 shows the pressure response to heat inputs of 200–250 W for a 95% liquid fill experiment. Before heat is applied, the working fluid is liquid in the lower section of the loop, and saturated vapor in the space at the top of the loop. As heat is added to the system, vapor bubbles are generated at the evaporator and rise to the top of the loop and to the condenser where they are condensed back into a liquid and release their latent heat. While the working fluid in the system is two-phase, the NPCHP operates as a TPLTS. When the system reaches the fully filled condition, i.e. all the working fluid is in the liquid phase and has expanded to completely fill the pipe, the pressure within the system begins to increase significantly. This occurs for the 250 W heat input in the 95% fill ratio experiment, as shown in Fig. 14. The system is not able to operate once it reaches the fully filled condition due to the rapid increase in pressure. Therefore, only low heat inputs (200 W or less) which do not allow the system to reach the fully filled condition are achievable for high fill ratio experiments where the working fluid can expand to fill the entire pipe.

For fill ratios lower than 95%, the system operates as a TPLTS. Not enough liquid fills the loop initially for the liquid to expand to fully fill the pipe without exceeding the maximum allowable temperature of the system. The heat transfer is achieved through release of latent heat as the working fluid is condensed into a liquid. Fig. 15 shows the 55% fill ratio experiment where the system operates as a TPLTS. The system pressure is slightly lower than saturation pressure at the heater, indicating the working fluid is vapor. At the BC of the loop, after the condenser, the saturation pressure is greater than the system pressure, indicating a compressed liquid at this location before again reaching the evaporator and transforming into a vapor.

The phases present throughout the experiment depend on the initial fill ratio and heating conditions. The NPCHP operates as a TPLTS for fill ratios less than 100% until the device reaches the fully filled condition and is no longer operational due to a rapid pressure rise, or a TPLTS if the fill ratio is not high enough for the liquid to expand to fill the entire pipe.

7. Conclusions

The NPCHP, as proposed by Lee et al., (2010a, 2010b) is not a new type of heat pipe, but exhibits characteristics of a TPLTS, and can be classified as such.

1. Before reaching the fully filled condition, or if the fill ratio is not high enough to reach the fully filled state from volume expansion, the NPCHP operates as a TPLTS. If the system reaches the fully filled condition, it can no longer operate.
2. The NPCHP has a high nominal effective thermal conductivity that is over 6000 times larger than that of copper. The NPCHP can transfer the same amount of heat, with a much smaller temperature difference between the evaporator and condenser, than a solid metal rod of comparable size.
3. The NPCHP can transport large quantities of heat through a small cross-sectional area over a considerable distance with no additional power input to the system with a small temperature drop.
4. The NPCHP has a fast thermal response time. A simulation of heat transfer through a copper rod is used to show that the NPCHP can transfer heat much faster than a high conductivity metal (copper).
5. The NPCHP can take in energy through a small surface area and expel the same amount of energy over a large surface area. The NPCHP has a thermal flux ratio between the heater and cooling jacket of approximately 11.
6. The NPCHP has a high heat flux on the order of 10^5 W/m^2, which is comparable to existing heat pipes of different types and material with similar effective length.

More experimental and numerical validation are needed to prove the effects of changing different system parameters of the NPCHP. Additional effort is needed to determine effects of changing heat input, working fluid, orientation in the gravitational field, and location of the heat source relative to the heat sink.

Declaration of Competing Interest

The authors declare that they have no known competing financial interests or personal relationships that could have appeared to influence the work reported in this paper.

Acknowledgement

This material is based upon work supported by the National Science Foundation under Grant No. 1744118 to the University of Connecticut and State Scholarship Fund from China Scholarship Council.

Appendix A. Supplementary material

Supplementary data to this article can be found online at https://doi.org/10.1016/j.ijheatmasstransfer.2019.118676.

References

[1] M.H. Beitelmal, C.D. Patel, *Two-Phase Loop, Compact Thermosyphon*, 2002.
[2] T.L. Bergman, A. Faghri, Review and Advances in Heat Pipe Analysis and Numerical Simulation, in: Numerical Simulation of Heat Exchangers, CRC Press, 2017, pp. 173–212.
[3] S. Boothaisong, S. Rittidech, T. Chompookham, M. Thongmoon, Y. Ding, Y. Li, Three-dimensional transient mathematical model to predict the heat transfer rate of a heat pipe, Adv. Mech. Eng. (2015), https://doi.org/10.1177/1687814014567811.
[4] S.W. Chang, D.C. Lo, K.F. Chiang, C.Y. Lin, Sub-atmospheric boiling heat transfer and thermal performance of two-phase loop thermosyphon, Exp. Therm. Fluid Sci. 39 (2012) 134–147, https://doi.org/10.1016/J.EXPTHERMFLUSCI.2012.01.017.
[5] A.A. Chehade, H. Louahlia-Gualous, S. Le Masson, I. Victor, N. Abouzahab-Damaj, Experimental investigation of thermosyphon loop thermal performance, Energy Convers. Manage. 84 (2014) 671–680, https://doi.org/10.1016/J.ENCONMAN.2014.04.092.
[6] R.T. Dobson, J.C. Ruppersberg, Flow and heat transfer in a closed loop thermosyphon. Part I – theoretical simulation, J. Energy Southern Africa 18 (3) (2007) 32–40.
[7] A. Faghri, Review and advances in heat pipe science and technology, J. Heat Transf. 134 (12) (2012), https://doi.org/10.1115/1.4007407 123001.
[8] A. Faghri, Heat pipes: review, opportunites and challenges, Front. Heat Pipes (FHP) 5 (2014) 1, https://doi.org/10.5098/fhp.5.1.
[9] A. Faghri, Heat Pipe Science and Technology, (2nd ed.)., Global Digital Press, 2016.
[10] A. Faghri, Heat Pipes and Thermosyphons, in: Handbook of Thermal Science and Engineering, 2017, pp. 1–50, https://doi.org/10.1007/978-3-319-26695-4_52.
[11] A. Faghri, Y. Zhang, Transport phenomena in multiphase systems, Elsevier Academic Press, 2006.
[12] A. Franco, S. Filippeschi, A. Franco, S. Filippeschi, S. Filippeschi, Closed loop two-phase thermosyphon of small dimensions: a review of the experimental results, Microgravity Sci. Technol. 24 (2012) 165–179, https://doi.org/10.1007/s12217-011-9281-6.
[13] W. Fu, X. Li, X. Wu, Z. Zhang, Investigation of a long term passive cooling system using two-phase thermosyphon loops for the nuclear reactor spent fuel pool, Ann. Nucl. Energy 85 (2015) 346–356, https://doi.org/10.1016/J.ANUCENE.2015.05.026.
[14] X. Han, X. Wang, H. Zheng, X. Xu, G. Chen, Review of the development of pulsating heat pipe for heat dissipation, Renew. Sustain. Energy Rev. 59 (2016) 692–709, https://doi.org/10.1016/j.rser.2015.12.350.
[15] Kang, S.-W., Tsai, M.-C., Hsieh, C.-S., & Chen, J.-Y. (2010). Thermal Performance of a Loop Thermosyphon.
[16] R. Khodabandeh, Pressure drop in riser and evaporator in an advanced two-phase thermosyphon loop, Int. J. Refrig. 28 (5) (2005) 725–734, https://doi.org/10.1016/J.IJREFRIG.2004.12.003.
[17] S. Lee, D. Yuan, B. Wu, Experimental Study on Non Phase Change Heat Pipe and its Mechanism Analysis, in: 20th National and 9th International ISHMT-ASME Heat and Mass Transfer Conference, 2010, pp. 1624–1630, https://doi.org/10.3850/9789810838133.
[18] S. Lee, D. Yuan, B. Wu, Experimental Study on the Counter-Gravity Effect of Non-Phase Change Heat Pipes, in: Proceedings of the 14th International Heat Transfer Conference, 2010, pp. 1–7.

[19] W.H. Lee, A Pressure Iteration Scheme for Two-Phase Flow Modeling, in: Multiphase Transport Fundamentals, Reactor Safety, Applications, 1980, p. 1.
[20] D. Lu, X. Zhang, C. Guo, Stability analysis for single-phase liquid metal rectangular natural circulation loops, Ann. Nucl. Energy 73 (2014) 189–199, https://doi.org/10.1016/J.ANUCENE.2014.06.014.
[21] M. Maiani, W.J.M. de Kruijf, W. Ambrosini, An analytical model for the determination of stability boundaries in a natural circulation single-phase thermosyphon loop, Int. J. Heat Fluid Flow 24 (6) (2003) 853–863, https://doi.org/10.1016/J.IJHEATFLUIDFLOW.2003.07.002.
[22] Y.F. Maydanik, Loop heat pipes, Appl. Therm. Eng. 25 (2005) 635–657, https://doi.org/10.1016/j.applthermaleng.2004.07.010.
[23] Y. Naresh, C. Balaji, Thermal performance of an internally finned two phase closed thermosyphon with refrigerant R134a: a combined experimental and numerical study, Int. J. Therm. Sci. 126 (2018) 281–293, https://doi.org/10.1016/J.IJTHERMALSCI.2017.11.033.
[24] K. Naveen, K.N. Iyer, J.B. Doshi, P.K. Vijayan, Investigations on single-phase natural circulation loop dynamics. Part 3: role of expansion tank, Prog. Nucl. Energy 78 (2015) 65–79, https://doi.org/10.1016/J.PNUCENE.2014.08.007.
[25] Y.J. Park, H.K. Kang, C.J. Kim, Heat transfer characteristics of a two-phase closed thermosyphon to the fill charge ratio, Int. J. Heat Mass Transf. 45 (23) (2002) 4655–4661, https://doi.org/10.1016/S0017-9310(02)00169-2.
[26] D.S. Pilkhwal, W. Ambrosini, N. Forgione, P.K. Vijayan, D. Saha, J.C. Ferreri, Analysis of the unstable behaviour of a single-phase natural circulation loop with one-dimensional and computational fluid-dynamic models, Ann. Nucl. Energy 34 (5) (2007) 339–355, https://doi.org/10.1016/J.ANUCENE.2007.01.012.
[27] L.M. Poplaski, A. Faghri, T.L. Bergman, Analysis of internal and external thermal resistances of heat pipes including fins using a three-dimensional numerical simulation, Int. J. Heat Mass Transf. 102 (2016) 455–469, https://doi.org/10.1016/j.ijheatmasstransfer.2016.05.116.
[28] V. Sankaran, C. Merkle, Comparison of Pressure-Based and Density-Based Methods for Low Mach, Number CFD Computations, 2004.
[29] M.M. Sarafraz, F. Hormozi, S.M. Peyghambarzadeh, Thermal performance and efficiency of a thermosyphon heat pipe working with a biologically ecofriendly nanofluid☆, Int. Commun. Heat Mass Transf. 57 (2014) 297–303, https://doi.org/10.1016/j.icheatmasstransfer.2014.08.020.
[30] Thermophysical Properties of Fluid Systems (2017).
[31] Z. Tong, X.-H. Liu, Z. Li, Y. Jiang, Experimental study on the effect of fill ratio on an R744 two-phase thermosyphon loop, Appl. Therm. Eng. 99 (2016) 302–312, https://doi.org/10.1016/J.APPLTHERMALENG.2016.01.065.
[32] P.K. Vijayan, Experimental observations on the general trends of the steady state and stability behaviour of single-phase natural circulation loops, Nucl. Eng. Des. 215 (1–2) (2002) 139–152, https://doi.org/10.1016/S0029-5493(02)00047-X.
[33] Volume of Fluid (VOF) Model Theory. (2006). Retrieved January 28, 2018, from https://www.sharcnet.ca/Software/Fluent6/html/ug/node880.htm.
[34] S. Wannapakhe, S. Rittidech, B. Bubphachot, O. Watanabe, Heat transfer rate of a closed-loop oscillating heat pipe with check valves using silver nanofluids as working fluid, J. Mech. Sci. Technol. (2009).
[35] P. Zhang, B. Wang, W. Shi, X. Li, Experimental investigation on two-phase thermosyphon loop with partially liquid-filled downcomer, Appl. Energy 160 (2015) 10–17, https://doi.org/10.1016/J.APENERGY.2015.09.033.
[36] Y. Zhang, A. Faghri, Advances and unsolved issues in pulsating heat pipes, Heat Transf. Eng. 29 (1) (2008) 20–44, https://doi.org/10.1080/01457630701677114.
[37] K. Smith, S. Siedel, A.J. Robinson, R. Kempers, The effects of bend angle and fill ratio on the performance of a naturally aspirated thermosyphon, Applied Thermal Engineering 101 (2016) 455–467, https://doi.org/10.1016/J.APPLTHERMALENG.2016.01.024.
[38] D. Sun, J. Xu, Q. Chen, Modeling of the Evaporation and Condensation Phase-Change Problems with FLUENT, Numerical Heat Transfer, Part B 66 (2014) 326–342, https://doi.org/10.1080/10407790.2014.915681.